
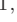





Neutron-Scattering Determination of Phonon Wave Function and Topological Invariant in Transition-Metal Monosilicides

Zhendong Jin,^{1, } Biaoyan Hu,^{1, } Yiran Liu,^{1, } Yangmu Li,² Tiantian Zhang,³ Kazuki Iida,⁴ Kazuya Kamazawa,⁴ A. I. Kolesnikov,⁵ M. B. Stone,⁵ Xiangyu Zhang,⁶ Haiyang Chen,⁶ Yandong Wang,⁶ I. A. Zaliznyak,² J. M. Tranquada,² Chen Fang,^{3, } and Yuan Li^{1,7, }

¹International Center for Quantum Materials, School of Physics, Peking University, Beijing 100871, China

²Condensed Matter Physics and Materials Science Division, Brookhaven National Laboratory, Upton, New York 11973, USA

³Beijing National Laboratory for Condensed Matter Physics, and Institute of Physics, Chinese Academy of Sciences, Beijing 100190, China

⁴Neutron Science and Technology Center, Comprehensive Research Organization for Science and Society (CROSS), Tokai, Ibaraki 319-1106, Japan

⁵Neutron Scattering Division, Oak Ridge National Laboratory, Oak Ridge, Tennessee 37831, USA

⁶State Key Laboratory for Advance Metals and Materials, University of Science and Technology Beijing, Beijing 10083, China

⁷Collaborative Innovation Center of Quantum Matter, Beijing 100871, China

(Dated: December 4, 2020)

In close analogy to electronic semimetals, a variety of Weyl, Dirac points and nodal lines are predicted for phonons recently by *ab initio* calculations, but very few experimental confirmations have been made. We performed Inelastic Neutron Scattering (INS) experiments on MnSi and CoSi crystals, and identified multiple types of unconventional Weyl and Dirac points in their Brillouin zone. Being aware of neutron scattering's capability of wavefunction detection and polarization determination, we further derived an explicit relation between the topological invariant of a Weyl node and the INS intensities nearby. Apart from protected surface states and novel transport phenomena, our work suggests that topological nodes also leave some observable traces in spectroscopic patterns.

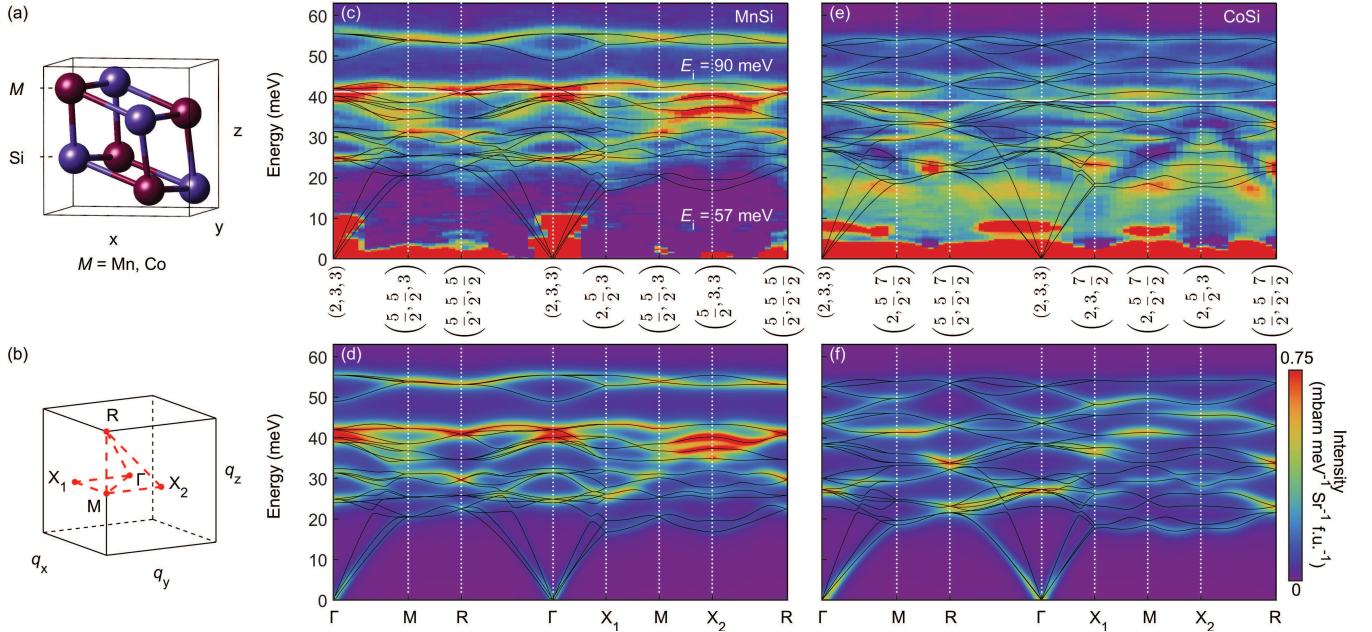


FIG. 1. Comparison between INS and calculated phonon spectra (a) Cubic primitive cell of MSi , with space group $P2_13$. (b) Corresponding Brillouin zone (BZ). High symmetry points are marked in red. (c),(e) Representative INS data of MnSi and CoSi along high symmetry lines. Raw data with $E_i = 57$ meV and 90 meV are aligned, while aluminum and incoherent signals are subtracted. (d),(f) Calculated $S(\mathbf{Q}, \omega)$ along the same momentum trajectories, using optimized parameter set. All measured and calculated intensities are displayed in the same absolute unit, benchmarked by Vanadium. Calculated band structures are shown together in thin black lines.

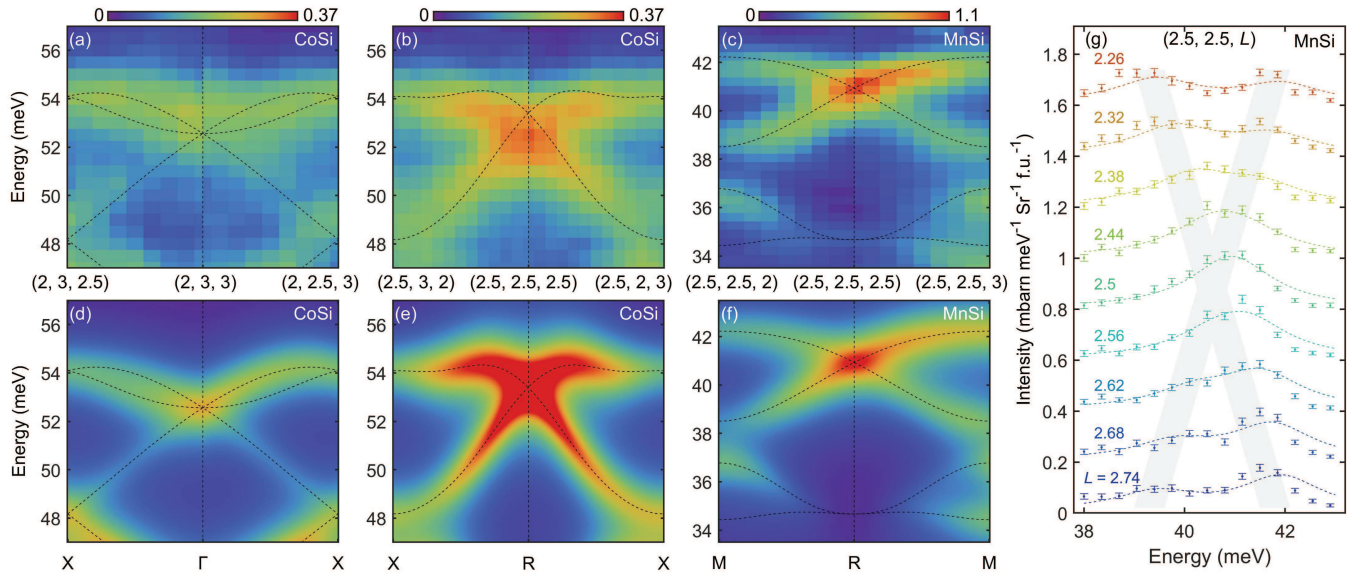


FIG. 2. Effective spin-1 Weyl and charge-2 Dirac phonons. (a) The spin-1 Weyl phonons at Γ point of CoSi, plotted along $X-\Gamma-X$ line. (b),(c) The charge-2 Dirac phonons at R points, plotted along $M-R-M$ direction for MnSi and $X-R-X$ for CoSi. All the bands are two-fold degenerated in these directions and exhibit linear features near R . (d)-(f) Calculated $S(\mathbf{Q}, \omega)$ on corresponding trajectories, in remarkable accordance with experiments. All measured and calculated intensities are displayed in the same units as in Fig. 1. (g) Intensity data points and DFPT-simulated curves taken along a series of \mathbf{Q} points. The peak positions show clear X-shape dispersions as indicated by the gray cross behind.

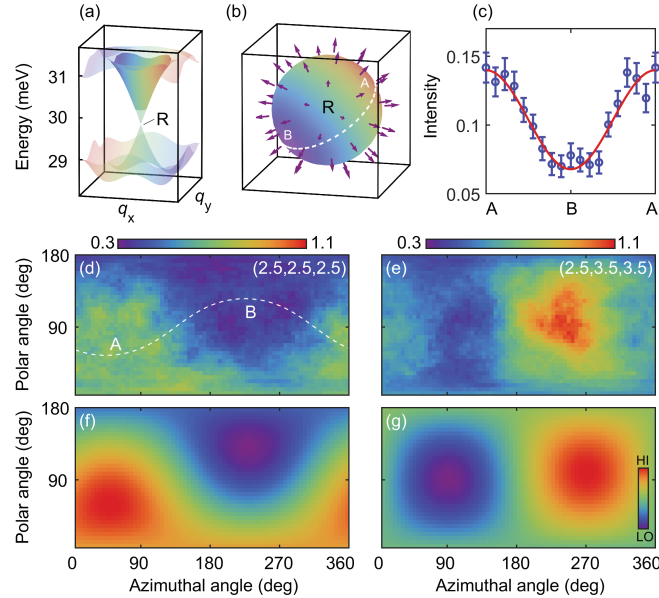


FIG. 3. Topological Properties of the Charge-2 Dirac points at R . (a) Band structure near the Charge-2 Dirac point at 29.6 meV in MnSi, shown together with energy integration range (30–32 meV). (b) The pseudospin \mathbf{S} texture on a \mathbf{q} -sphere enclosing R , together with the illustration of INS intensity near $\mathbf{Q} = (2.5, 2.5, 2.5)$. (c) Experimental results along the white loop ABA marked in (b). The red line is a cosine fit. (d),(e) INS intensity on the spheres enclosing $(2.5, 2.5, 2.5)$ and $(2.5, 3.5, 3.5)$ respectively, with radius $|\mathbf{q}| = 0.2$ r.l.u. and smooth width 20° . (e),(f) Theoretical predictions by calculating projection of pseudospin \mathbf{S} onto the direction of \mathbf{V} .

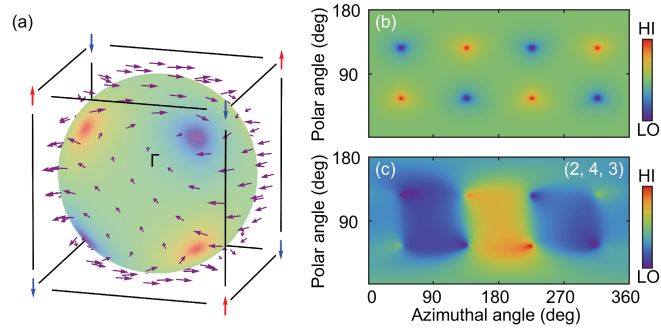


FIG. 4. Topological Properties of the Quadruple Weyl points at Γ . (a) The pseudospin \mathbf{S} texture on a \mathbf{q} -sphere enclosing Γ , with the colors further indicating the S_z component. The orientations of \mathbf{S} at 8 diagonal directions are marked specially by blue and red arrows, showing Tetrahedral symmetry. (b) S_z component of the pseudospin, in a world-map fashion. (c) Simulated INS intensity near $\mathbf{Q} = (2, 4, 3)$, where \mathbf{V} is almost in z direction. All simulations are done with $|\mathbf{q}| = 0.05$ and realistic coefficients of (the upper band of) the 40.1 meV band-crossing in MnSi.

* These authors contributed equally to this study.

† cfang@iphy.ac.cn

‡ yuan.li@pku.edu.cn

Neutron-Scattering Determination of Phonon Wave Function and Topological Invariant in Transition-Metal Monosilicides: Supplementary Material

Zhendong Jin,^{1, *} Biaoyan Hu,^{1, *} Yiran Liu,^{1, *} Yangmu Li,² Tiantian Zhang,³ Kazuki Iida,⁴ Kazuya Kamazawa,⁴ A. I. Kolesnikov,⁵ M. B. Stone,⁵ Xiangyu Zhang,⁶ Haiyang Chen,⁶ Yandong Wang,⁶ I. A. Zaliznyak,² J. M. Tranquada,² Chen Fang,^{3, †} and Yuan Li^{1, 7, ‡}

¹International Center for Quantum Materials, School of Physics, Peking University, Beijing 100871, China

²Condensed Matter Physics and Materials Science Division, Brookhaven National Laboratory, Upton, New York 11973, USA

³Beijing National Laboratory for Condensed Matter Physics, and Institute of Physics, Chinese Academy of Sciences, Beijing 100190, China

⁴Neutron Science and Technology Center, Comprehensive Research Organization for Science and Society (CROSS), Tokai, Ibaraki 319-1106, Japan

⁵Neutron Scattering Division, Oak Ridge National Laboratory, Oak Ridge, Tennessee 37831, USA

⁶State Key Laboratory for Advance Metals and Materials, University of Science and Technology Beijing, Beijing 10083, China

⁷Collaborative Innovation Center of Quantum Matter, Beijing 100871, China

(Dated: December 4, 2020)

* These authors contributed equally to this study.

† cfang@iphy.ac.cn

‡ yuan.li@pku.edu.cn

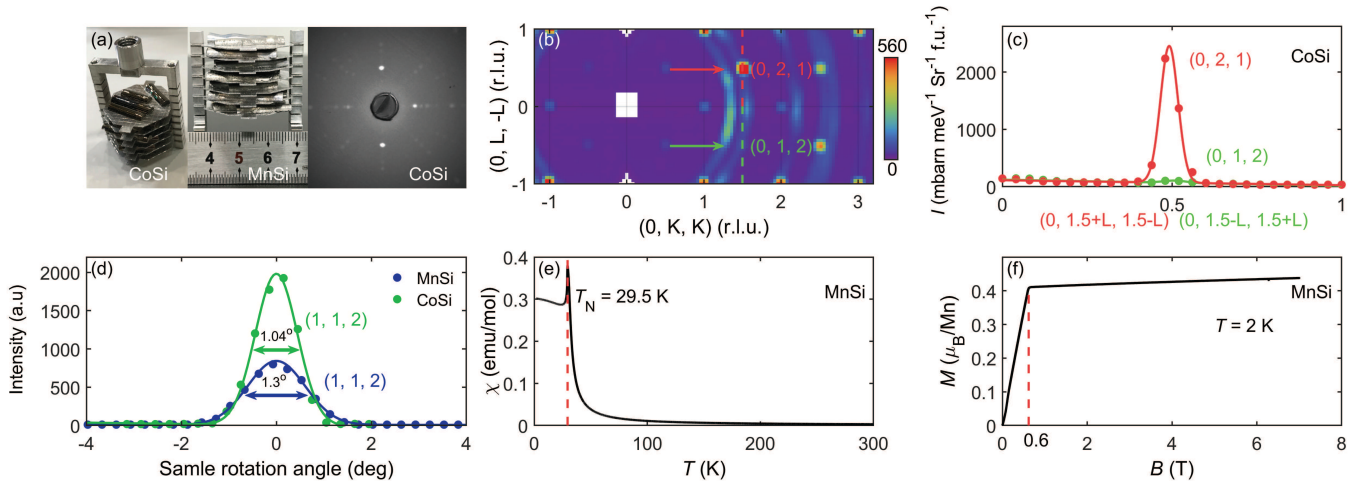


FIG. S1. Sample preparation and characterization. (a) Left: CoSi (28 g) and MnSi (33 g) single crystals, grown by a travelling-solvent floating zone method and co-aligned on aluminum sample holders. Right: X-ray diffraction pattern of single crystal CoSi along [100] direction. (b), (c) The (0, 2, 1) Bragg peak of CoSi is > 25 times higher than the (0, 1, 2) peak, suggesting that the crystal array in (a) are effectively single-domained. (d) Neutron diffraction intensity of the (1, 1, 2) Bragg peaks. The FWHMs are 1.04° for CoSi and 1.3° for MnSi, indicating perfect crystal alignment and small mosaic spread. (e), (f) Magnetic moment of single crystal MnSi measured by MPMS. A (helical) antiferromagnetic order formed below $T_N = 29.5$ K, with a saturated moment of $\sim 0.4 \mu_B$ per Mn atom at $B > 0.6$ T, in consistent with previous reports.

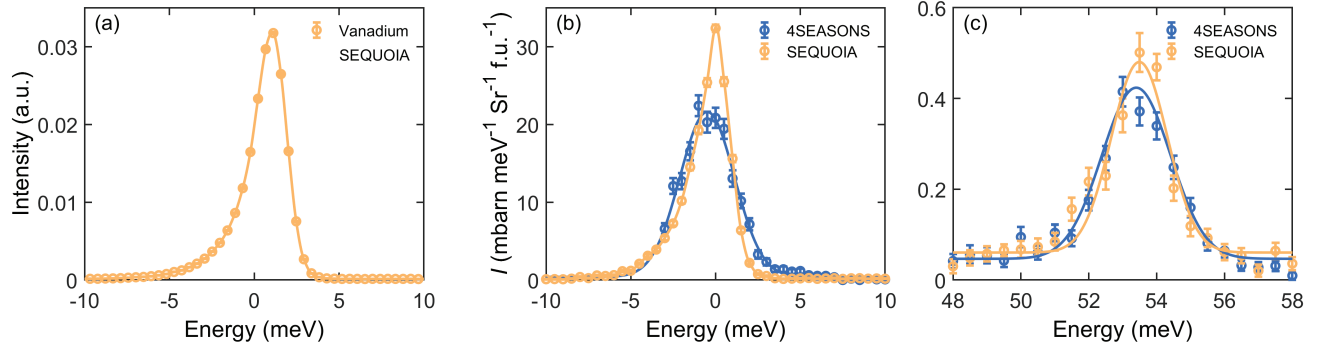


FIG. S2. Intensity calibration. (a) Calibration at SEQUOIA was done by measuring the elastic scattering intensity of standard Vanadium sample. (b) The SEQUOIA and 4SEASONS data are further aligned so that the integrated area below the elastic peaks are the same. (c) INS data of MnSi obtained at SEQUOIA and 4SEASONS shown together, near an optical phonon branch at $\mathbf{Q} = (1.5, 2.5, 2.5)$, $E = 53.7$ meV. All data points in (a), (b) and (c) are taken with $E_i = 90$ meV.

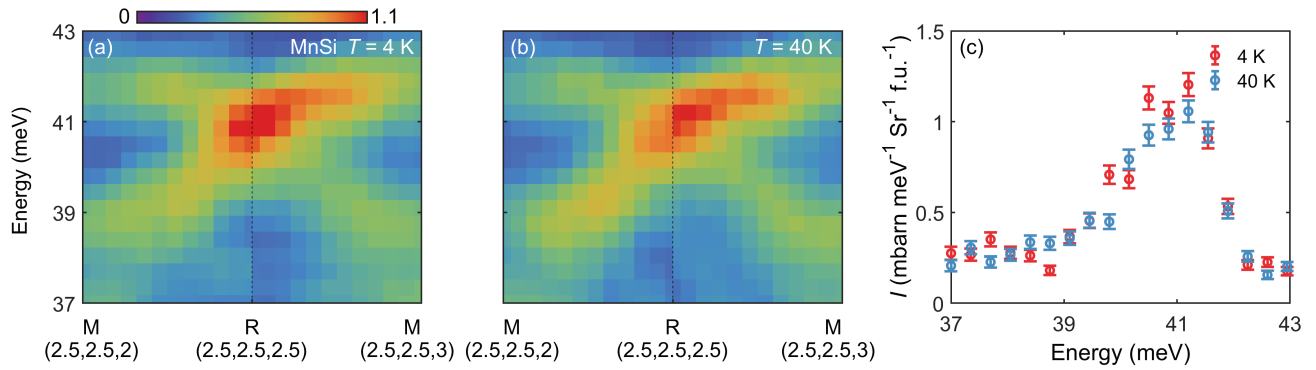


FIG. S3. Magnetic effects on phonon spectra. (a), (b) INS intensity of MnSi along M-R-M directions, measured at $T = 4$ K and 40 K respectively ($E_i = 57$ meV). (c) Energy scan at $\mathbf{Q} = (2.5, 2.5, 2.5)$, showing no significant change in intensity. Having checked many different BZs, we conclude that the magnetic order of MnSi below $T_N = 29.5$ K has little effects on its phonon spectra.

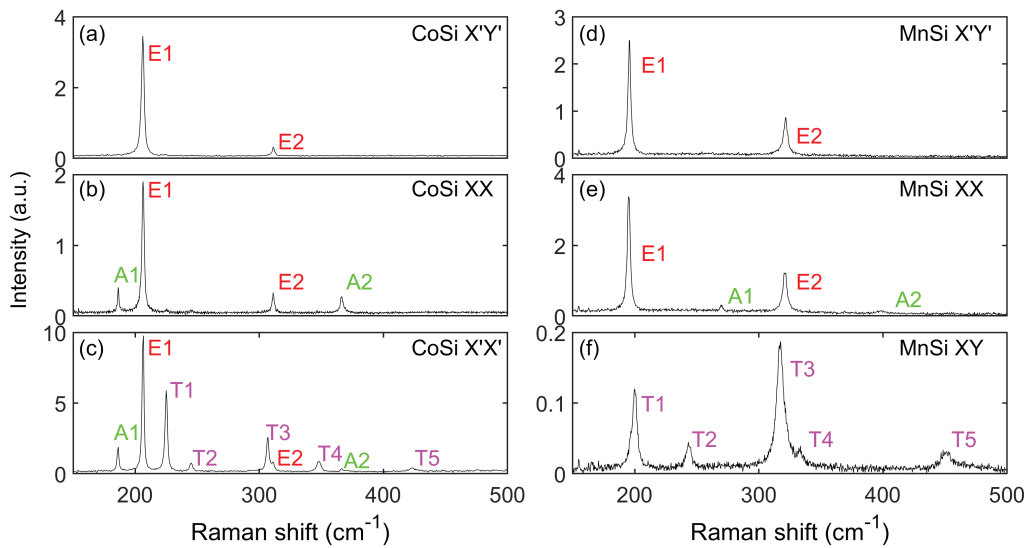


FIG. S4. Raman spectra of phonons in CoSi and MnSi. The A, E, T irreps are identified by utilizing different polarizations, so as to confirm the degeneracy of each band-crossing at Γ . $X'Y'$ directions are in 45° angle with XY .

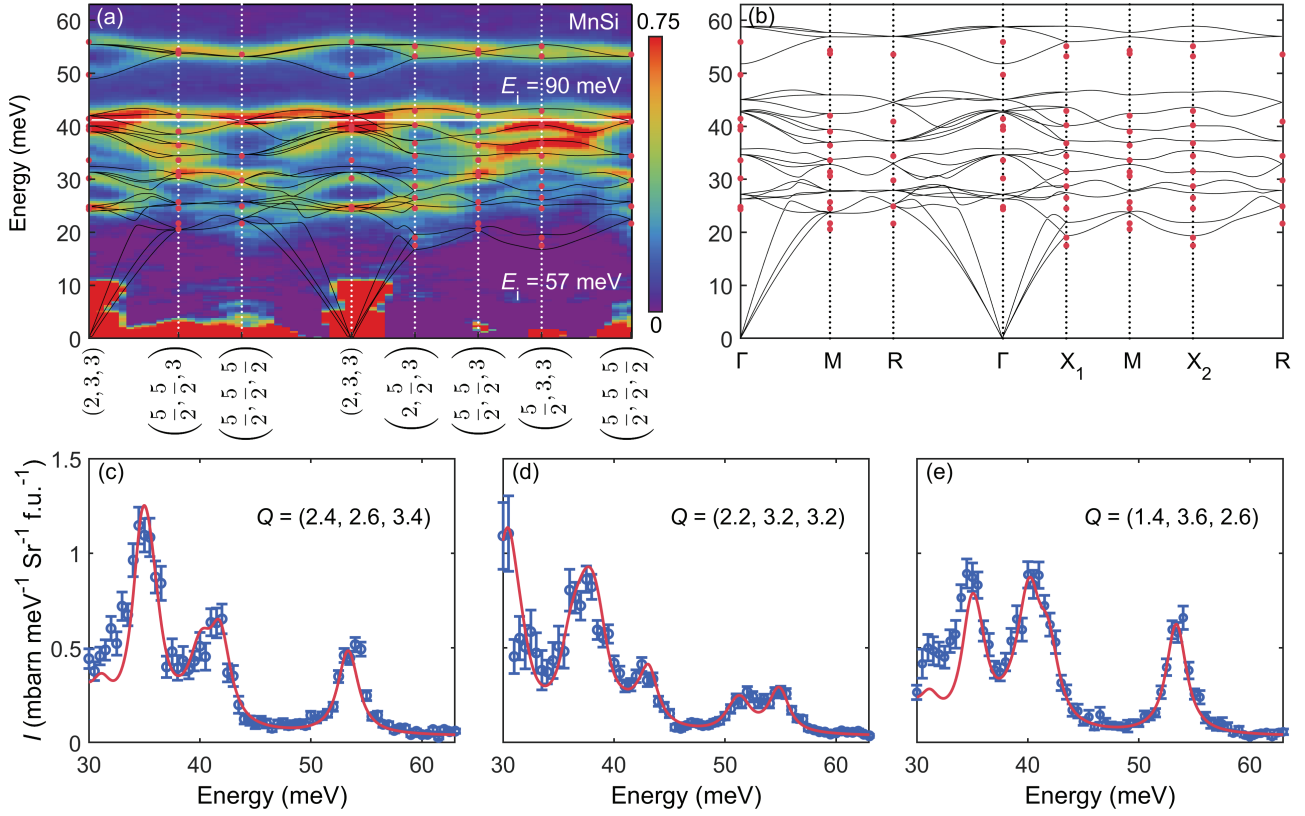


FIG. S5. Band structure fits for MnSi (a) Phonon energies of all bands at Γ , X , M , R are extracted from INS spectra (red dots). The black lines illustrate optimized band structures, in good agreement with INS results. (b) Unadjusted band structures from DFPT outputs, with significant difference with experiments. (c)-(e) Measured and fitted INS intensities at selected Q -points, showing remarkable accordance.

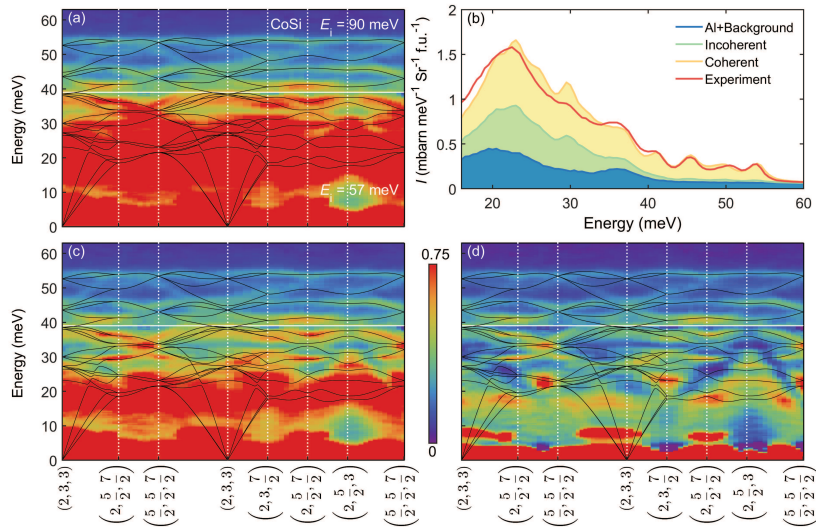


FIG. S6. Intensity fits for CoSi. (a) Raw INS intensity data of CoSi along high symmetry directions. (b) Averaged INS intensity over the $(2, 3, 3)$ BZ. The fitted coherent, incoherent and aluminum (with background) scattering intensities are shown respectively. (c) Enhanced INS intensity data after subtracting incoherent signals. (d) Best estimate of coherent intensity along the chosen trajectory, obtained by subtracting both incoherent and aluminum signals.